Super-Resolution UWB Radar Imaging Algorithm Based on Extended Capon with Reference Signal Optimization

Shouhei Kidera*, Takuya Sakamoto† and Toru Sato†
* Dept. of Electronic Engineering, University of Electro-Communications, Tokyo, JAPAN,
Email: kidera@ee.uec.ac.jp
† Graduate School of Informatics, Kyoto University, Kyoto, JAPAN

***Abstract*—Near field radar employing UWB (Ultra Wideband) signals with its high range resolution provides various sensing applications. It enables a robotic or security sensor that can identify a human body even in invisible situations. As one of the most efficient radar algorithms, the RPM (Range Points Migration) is proposed. This achieves fast and accurate estimating shapes of surfaces, even for complex-shaped targets by eliminating the difficulty of connecting range points. However, in the case of a complicated target surface whose variation scale is less than wavelength, it still suffers from image distortion caused by multiple interference signals mixed together by different waveforms. As a substantial solution, this paper proposes a novel range extraction algorithm by extending the Capon, known as FDI (Frequency Domain Interferometry). This algorithm combines reference signal optimization with the original Capon method to enhance the accuracy and resolution for an observed range into which a deformed waveform model is introduced. The result obtained from numerical simulation proves that super-resolution UWB radar imaging is accomplished by the proposed method, even for an extremely complex-shaped targets including edges.**

I. Introduction

UWB pulse radar with high range resolution promise for various sensing techniques especially for the near field. This radar is applicable to non-contact measurement for reflector antennas or aircraft bodies that have specular surfaces, or to robotic sensors that can identify a human body, even in a blurry vision such as a dark smog in disaster areas. In addition, it is suitable for surveillance or security systems for intruder detection or aged care, where an optical camera has the serious problem of privacy invasion in the case for living places. While many kinds of radar algorithms have been developed [1]–[3], they are still inappropriate for the above applications because of a large amount of calculation time or inadequate image resolution. Accepting the problems occurs in conventional techniques, a number of radar imaging algorithms have been already proposed, which accomplish a real-time and high resolution surface extraction beyond wavelength [4]–[6]. As a high-speed and accurate surface estimating method applicable to various target boundaries, the RPM algorithm has been proposed [7]. This algorithm directly estimates an accurate DOA (Direction Of Arrival) with a global characteristic of observed range points, avoiding the difficulty in connecting range points. The RPM is based on a simple idea, yet, it offers an accurate target surface including the complex-shaped target that principally creates an extremely complicated range map.

However, this algorithm suffers from a serious image distortion, in the case of more complicated target which has a surface variation less than wavelength or has many convex and concave edges. This distortion is caused by the richly interfered signals scattered from the multiple scattering centers on the target surface. These components are received within a range scale smaller than wavelength, and are hardly separated by the conventional range extraction methods, such as the Wiener filter.

To overcome this difficulty, this paper proposes a novel range extraction algorithm by extending the Capon method. While the Capon is useful for enhancing the range resolution based on the FDI [8], the resolution and accuracy of this method significantly depend on a reference waveform such as transmitted wave. In general, the scattered waveform from the target with wavelength scale differs from the transmitted one [9], and the range resolution given by the original Capon method deteriorates due to this deformation. To outperform the original Capon, this paper extends the original Capon so that it optimizes the reference signal using the simplified waveform model. The optimized reference signal significantly enhances the range resolution and accuracy of the Capon, and brings out the utmost performance of the RPM algorithm. The result obtained from numerical simulation verifies that the proposed algorithm combining the RPM and the extended Capon accomplishes a super-resolution imaging, where a complex-shaped surface with edges is accurately extracted.

II. System Model

Fig. 1 shows the system model in the 2-dimensional model. It assumes the mono-static radar, and an omni-directional antenna is scanned along the x-axis. It is assumed that the target has an arbitrary shape with a clear boundary. The propagation speed of the radio wave c is assumed to be known constant. A mono-cycle pulse is used as the transmitting current. The real space in which the target and antenna are located, is expressed by the parameters (x, z). The parameters are normalized by λ, which is the central wavelength of the pulse. $z > 0$ is assumed for simplicity. $s'(X, Z')$ is defined as the received electric field

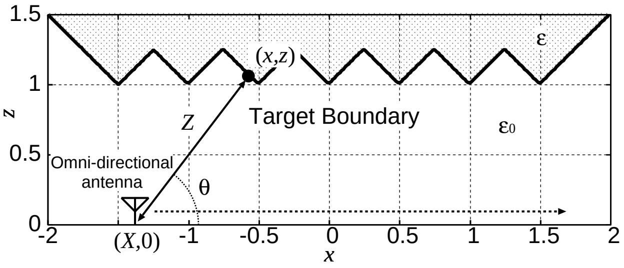

Fig. 1. System model.

at the antenna location $(x, z) = (X, 0)$, where $Z' = \mathrm{c}t/(2\lambda)$ is a function of time t.

III. RPM Algorithm

Various kinds of radar imaging algorithms based on an aperture synthesis, time reversal or range migration methods, have been proposed [1]–[3]. As the real-time imaging algorithm, the SEABED has been developed, which uses a reversible transform BST (Boundary Scattering Transform) between the observed ranges and the target boundary [4]. In addition, another high-speed imaging algorithm termed Envelope has been developed aiming at enhancing the image stability of SEABED, by avoiding the range derivative operations [5], [6]. While these algorithms accomplish real-time and high-resolution imaging for a simple shaped object, such as trapezoid, pyramid or sphere shapes, it is hardly applicable to a complex-shaped or multiple targets because they both require correctly connected range points.

As one of the most promising algorithm applicable to various target shapes, the RPM algorithm has been proposed [7]. This assumes that a target boundary point (x, z) exists on a circle with center $(X, 0)$ and radius Z, and then employs an accurate DOA (shown as θ in Fig. 1) estimation by making use of the global characteristics of the observed range map. The optimum $\theta_{\rm opt}$ is calculated as

$$\theta_{\rm opt}(\boldsymbol{q}) = \arg \max_{0\le\theta\le\pi} \left| \sum_{i=1}^{N_{\rm q}} s(\boldsymbol{q}_i) \quad \mathrm{e}^{-\left\{ \frac{(X-X_i)^2}{2\sigma_X^2} + \frac{(\theta-\theta(\boldsymbol{q},\boldsymbol{q}_i))^2}{2\sigma_\theta^2} \right\}} \right|, \tag{1}$$

where $\boldsymbol{q} = (X, Z)$, $\boldsymbol{q}_i = (X_i, Z_i)$ and and $N_{\rm q}$ is the number of the range points. $\theta(\boldsymbol{q}, \boldsymbol{q_i})$ denotes the angle from the x axis to the intersection point of the circles, with parameters (X, Z) and (X_i, Z_i). The constants σ_θ and σ_X are empirically determined. The detail of this algorithm is described as in [7]. The target boundary (x, z) for each range point (X, Z) is expressed as $x = X + Z\cos\theta_{\rm opt}(\boldsymbol{q})$ and $z = Z\sin\theta_{\rm opt}(\boldsymbol{q})$. This algorithm ignores range points connection and produces accurate target points, even if an extremely complicated range distribution is given. Thus, the inaccuracy occurring in the SEABED and Envelope, can be substantially avoided using this method. Fig. 2 shows the example of the RPM under the assumption that the true range points are given as in the upper side of this figure. Here, $s(\boldsymbol{q}) = 1.0$ is set for simplicity. The lower side of Fig. 2 shows a distinct advantage for this algorithm that it accurately locates the target points, even if the complex-shaped target is assumed.

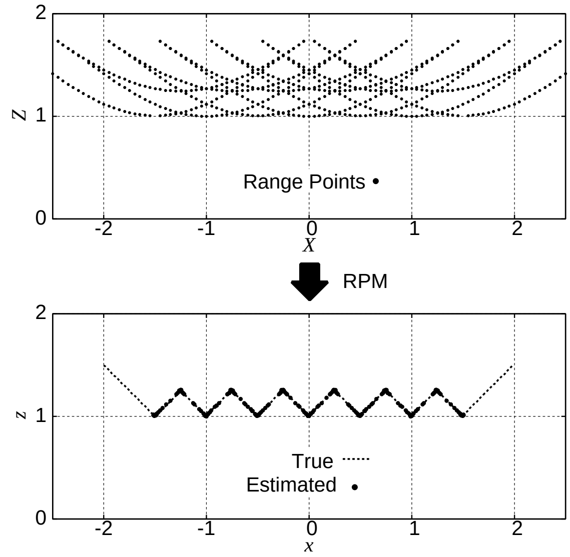

Fig. 2. True range points (upper) and extracted target points with RPM (lower).

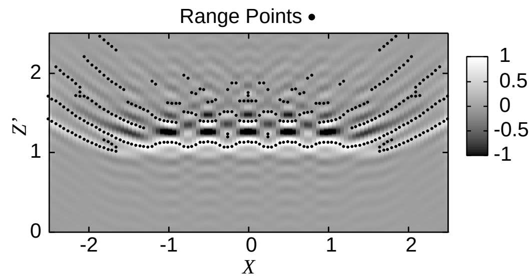

Fig. 3. Output of Wiener filter and extracted range points.

The performance example of RPM is presented here, where the received electric field is calculated by the FDTD (Finite Difference Time Domain) method. The former study [7] employs the Wiener filter in order to extract an range point for each location. The range points (X, Z) are extracted from the peaks of $s(X, Z')$ which are beyond the determined threshold. Fig. 3 shows the output of the Wiener filter, and the extracted range points, where the target boundary is assumed as in Fig. 1. The received signals are calculated at 101 locations between $-2.5 \le X \le 2.5$. A noiseless environment is assumed. Fig. 4 presents the comparison between the true and extracted range points in this case. It shows that the range points suffer from the inaccuracy caused by the peak shift of $s(X, Z')$ due to the multiple interfered signals within a range scale less than wavelength. Fig. 5 shows the target points, when the RPM is applied to the range points in Fig. 4. This figure indicates that the inaccuracy of range points distorts the target image, which is totally inadequate for identifying the

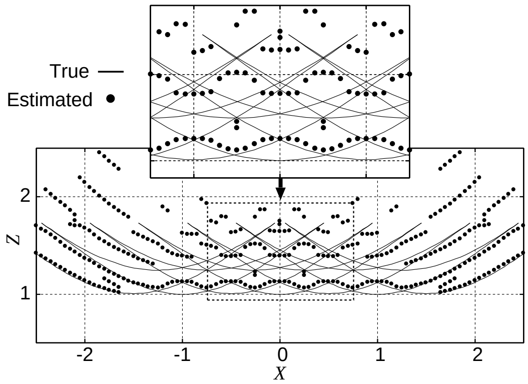

Fig. 4. Extracted range points with Wiener filter.

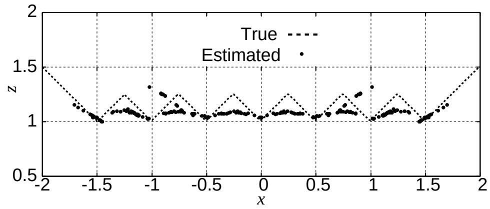

Fig. 5. Estimated target points with RPM and the Wiener filter.

target shape, especially for the target sides or concave edges. In addition, these ranges include small errors caused by deformed scattered waves, whose characteristics are detailed in [9].

To enhance the accuracy for range points extraction, the SOC (Spectrum Offset Correction) algorithm has been developed aiming at compensating the range shift due to the waveform deformation [6]. It is, however, confirmed that the range accuracy of the SOC is entirely inadequate in such as richly interfered situation. This is because the range errors in this case are dominantly caused by the peak shift of the Wiener filter due to the interference of multiple scattering echoes. Furthermore, the SOC is based on the center periods estimation of the scattered signal, when each signal should be correctly resolved in the time domain. This is, however, difficult when the multiple interfered signals are mixed together in a time scale less than its center period.

IV. Proposed Range Extraction Algorithm

To overcome the difficulty described above, this paper proposes a novel algorithm for range points extraction, by extending the Capon method. The Capon algorithm is one of the most powerful tools for enhancing range resolution based on FDI. It is confirmed, however, that the scattered waveform deformation distorts the range resolution and accuracy of the original Capon method. As a solution for this, the proposed method optimizes the reference signal used in the Capon. This method introduces a reference waveform model, based on the fractional derivative of the transmitted waveform as,

$$S_{\rm ref}(\omega,\alpha) = ({\rm j}\omega)^{\alpha} S_{\rm tr}(\omega)^{*}, \quad (2)$$

where $S_{\rm tr}(\omega)$ is the angular frequency domain of the transmitted signal and * denotes a complex conjugate. α is a variable

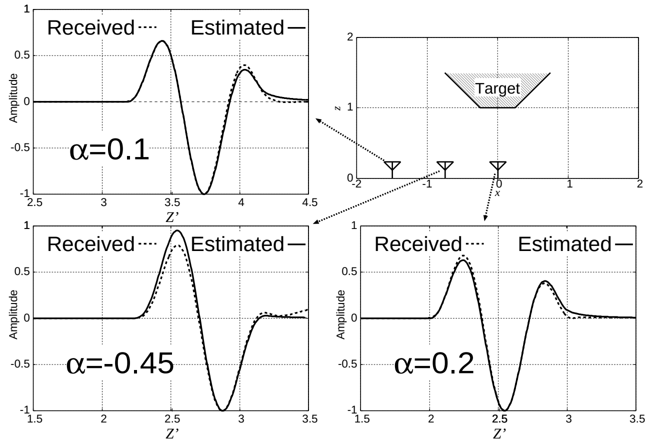

Fig. 6. Waveform comparison for each antenna location in polygonal target.

which satisfies $|\alpha| \le 1$.

The waveform comparison using this simplified model is demonstrated as follows. Fig. 6 shows the scattered waveform from the polygonal target received at the different locations, and the estimated waveforms with the optimized α in Eq. (2). This figure indicates that a scattered waveform differs depending on antenna location, or a local shape around the scattering center [9]. This deformation distorts the resolution and accuracy of the original Capon method, because it employs a phase and amplitude interferometry in each frequency between the reference and scattered waveforms. Fig. 6 also shows that each estimated waveform with the optimized α accurately approximates an actual deformed waveform, where the range accuracy is estimated within 0.01 λ when using the matched filter.

Based on this waveform model, the observed vector $\boldsymbol{V}_n(\alpha,\boldsymbol{L})$ is defined as,

$$\boldsymbol{V}_n(\alpha,\boldsymbol{L}) = \left[\frac{S(\omega_n,\boldsymbol{L})}{S_{\rm ref}(\omega_n,\alpha)},\cdots,\frac{S(\omega_{n+M-1},\boldsymbol{L})}{S_{\rm ref}(\omega_{n+M-1},\alpha)}\right]^T, \quad (3)$$

where $S(\omega,\boldsymbol{L})$ denotes the received signal in angular frequency domain at $\boldsymbol{L}=(X,0)$, and M denotes the dimension of $\boldsymbol{V}_n(\alpha,\boldsymbol{L})$. Here, in order to suppress a range sidelobe caused by the coherent interference signals, the frequency averaging is used. The averaged correlation matrix $\boldsymbol{R}(\alpha,\boldsymbol{L})$ is defined as,

$$\boldsymbol{R}(\alpha,\boldsymbol{L}) = \sum_{n=1}^{N-M+1} z_n \boldsymbol{V}_n(\alpha,\boldsymbol{L})\boldsymbol{V}_n^H(\alpha,\boldsymbol{L}), \quad (4)$$

where ^{H} denotes the Hermitian transpose. N is the total number of the frequency points, and determined by the maximum frequency band of the transmitted signal $S_{\rm tr}(\omega)$. $M \le N$ holds. z_n is defined by $z_n = 1/(N-M+1)$ for simplicity. The output of the extended Capon $s_{\rm cp}(\alpha,Z',\boldsymbol{L})$ is defined as,

$$s_{\rm cp}(\alpha,Z',\boldsymbol{L}) = \frac{S_0^{-1}}{\boldsymbol{a}^H(Z')\boldsymbol{R}(\alpha,\boldsymbol{L})^{-1}\boldsymbol{a}(Z')}, \quad (5)$$

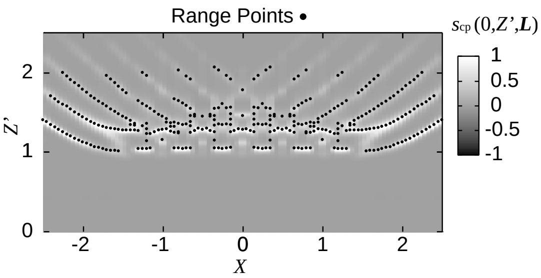

Fig. 7. Output of the original Capon method and extracted range points.

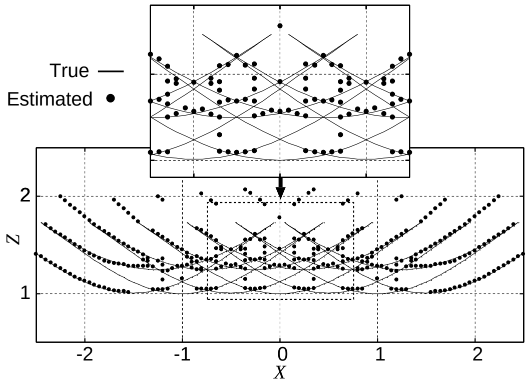

Fig. 8. Comparison between the true and extracted range points with the original Capon method.

where $\boldsymbol{a}(Z')$ denotes the steering vector of Z' for each frequency,

$$\boldsymbol{a}(Z') = \left[\mathrm{e}^{-\mathrm{j}\omega_1 2Z'\lambda/\mathrm{c}}, \mathrm{e}^{-\mathrm{j}\omega_2 2Z'\lambda/\mathrm{c}}, ..., \mathrm{e}^{-\mathrm{j}\omega_M 2Z'\lambda/\mathrm{c}}\right]^T, \quad (6)$$

S_0 is defined as

$$S_0 = \sqrt{\int \left\{\boldsymbol{a}^H(Z')\boldsymbol{R}(\alpha,\boldsymbol{L})^{-1}\boldsymbol{a}(Z')\right\}^{-2} \mathrm{d}Z'}. \quad (7)$$

The normalization with S_0 enables us to compare the amplitude of $s_{\mathrm{cp}}(\alpha, Z', \boldsymbol{L})$ with respect to α. Then, the local maximum of $s_{\mathrm{cp}}(\alpha, Z', \boldsymbol{L})$ for α and Z' offers an optimized range resolution in the Capon method. Finally, it determines the range points (X, Z), which satisfies the following conditions,

$$\left.\begin{array}{c} \partial s_{\mathrm{cp}}(\alpha, Z', \boldsymbol{L})/\partial\alpha = 0 \\ \partial s_{\mathrm{cp}}(\alpha, Z', \boldsymbol{L})/\partial Z' = 0 \\ s_{\mathrm{cp}}(\alpha, Z', \boldsymbol{L}) \geq \max\limits_{Z'} \beta s_{\mathrm{cp}}(\alpha, Z', \boldsymbol{L}) \end{array}\right\},$$

where β is empirically determined. This algorithm selects an accurate range point by enhancing the range resolution of the Capon method with the optimized reference signal. Each target point (x, y, z) is calculated from the group of range points in Eq. (1), that is the RPM.

A. Performance evaluation in numerical simulation

This section presents the examples for each range extraction method, where the same data as in Fig. 3 is used. Fig. 7 shows the output of the original Capon method and the extracted

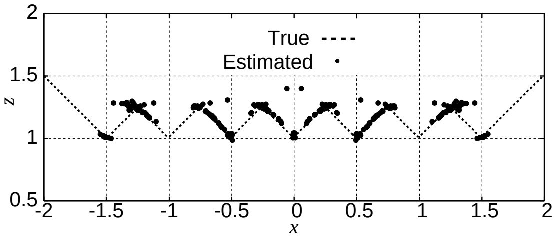

Fig. 9. Estimated target points with RPM and the original Capon method.

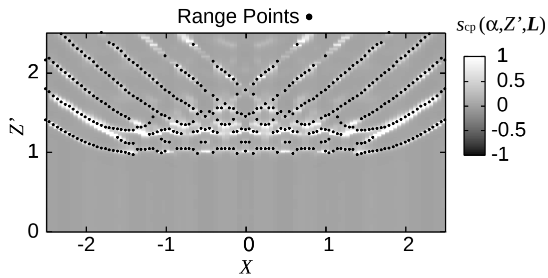

Fig. 10. Output of the extended Capon method and extracted range points.

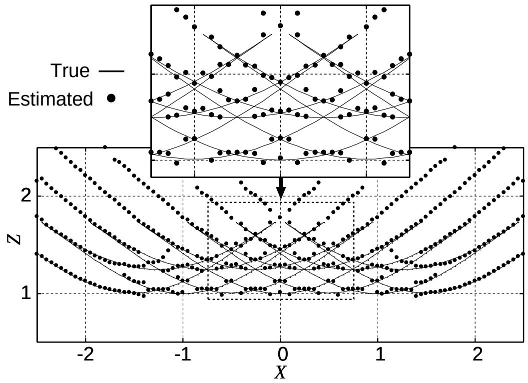

Fig. 11. Comparison between the true and extracted range points with the extended Capon method.

range points, which corresponds to $\alpha = 0$ in Eq. (8), i. e. the waveform deformation is not considered in this case. Fig. 8 shows the comparison between the true and extracted range points in this case. Here, $N = 60$, $M = 20$ and $\beta = 0.3$ are set. In this figure, the number of the accurate range points increases because the original Capon enhances the range resolution. Fig. 9 shows the estimated target points by using the original Capon method. This figure also shows that it enhances the accuracy of the location of imaging points, and the target points are accurately located around the target sides and edges. However, an inaccuracy around the concave edge region is recognized, and some parts of the target boundary are still not reconstructed. This is because of the distorted resolution and accuracy of ranges caused by the reference and actual scattered waveform being in-coincidence.

On the contrary, Fig. 10 shows $s_{\mathrm{cp}}(\alpha, Z', \boldsymbol{L})$ with the optimized α, and the range points extracted. Fig. 11 offers the same view in Fig. 8 in this case. This figure verifies that the extracted range points are accurately located, and the number

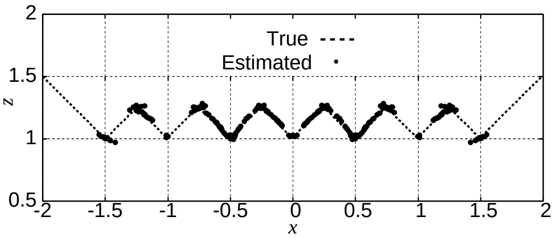

Fig. 12. Estimated target points by using the proposed method.

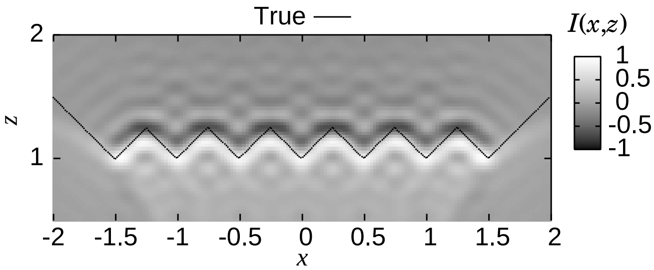

Fig. 13. Estimated image with the SAR.

of accurate range points increases compared with the original Capon method. Fig. 12 shows the estimated target points obtained by the RPM. This figure shows these points accurately reconstruct the convex or concave edge region, and offer a substantial information for identifying the complicated target shape, even with convex or concave edges. This is because the proposed method enhances the resolution of $s_{\rm cp}(\alpha, Z', \boldsymbol{L})$ with respect to the scattered waveform deformation. Thereby, the peaks embedded, which are regarded as the trivial value in the output of the original Capon, can be detected by optimizing the reference waveform.

As the comparison for the other methods not specified to the clear boundary extraction, the SAR (Synthetic Aperture Radar) method is introduced. This algorithm is the most useful for radar imaging [1], and the near field extension is applied here [7]. Fig. 13 shows the example of the SAR. While the image produced by the SAR is stable, its spatial resolution is substantially inadequate for recognizing the concave or convex edges. This result also proves the advantage for the proposed method, in terms of high-resolution imaging.

Here, the quantitatively analysis is introduced by ϵ as

$$\epsilon(\boldsymbol{x}_{\rm e}^i) = \min_{\boldsymbol{x}} \|\boldsymbol{x} - \boldsymbol{x}_{\rm e}^i\|, \quad (i = 1, 2, ..., N_{\rm T}), \tag{8}$$

where $\boldsymbol{x}$ and $\boldsymbol{x}_{\rm e}^i$ express the location of the true target point and that of the estimated target points, respectively. $N_{\rm T}$ is the total number of $\boldsymbol{x}_{\rm e}^i$. Fig. 14 plots the number of the estimated points for each value of ϵ. This figure verifies that the number of the accurate target points significantly increases, compared with other conventional algorithms. The mean values ϵ for each method are $5.66 \times 10^{-2}\lambda$ for the Wiener filter, $2.18 \times 10^{-2}\lambda$ for the original Capon, and $1.23 \times 10^{-2}\lambda$ for the proposed method. This result quantitatively proves the effectiveness of the proposed range extraction algorithm. Furthermore, it is

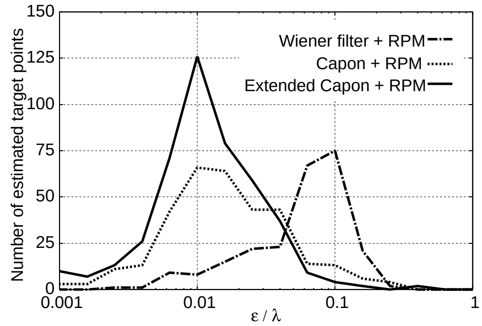

Fig. 14. Number of the target points for each ϵ.

confirmed that the accuracy can be held to within $5.0 \times 10^{-2}\lambda$, if the S/N ≥ 40 dB is obtained.

V. Conclusion

This paper proposed a novel range extraction algorithm as the extended Capon method, known as the frequency domain interferometry. To enhance the image quality of the RPM, including the case for complicated shaped objects with concave or convex edges, this method extends the original Capon so that it optimizes the reference signal with a simplified waveform model. It has a substantial advantage that the range resolution is remarkably enhanced, even if the different scattered waves are mixed together within the range scale less than wavelength. The result from numerical simulation verified that the combination with the extended Capon and RPM significantly improved the accuracy for the boundary extraction for the complex-shaped targets with edges.

References

[1] D. L. Mensa, G. Heidbreder and G. Wade, “Aperture Synthesis by Object Rotation in Coherent Imaging,” *IEEE Trans. Nuclear Science.*, vol. 27, no. 2, pp. 989–998, Apr, 1980.

[2] D. Liu, G. Kang, L. Li, Y. Chen, S. Vasudevan, W. Joines, Q. H. Liu, J. Krolik and L. Carin, “Electromagnetic time-reversal imaging of a target in a cluttered environment,” *IEEE Trans. Antenna Propagat.*, vol. 53, no. 9, pp. 3058–3066, Sep, 2005.

[3] F. Soldovieri, A. Brancaccio, G. Prisco, G. Leone and R. Pieri, “A Kirchhoff-Based Shape Reconstruction Algorithm for the Multimonostatic Configuration: The Realistic Case of Buried Pipes,” *IEEE Trans. Geosci. Remote Sens.*, vol. 46, no. 10, pp. 3031–3038, Oct, 2008

[4] T. Sakamoto and T. Sato, “A target shape estimation algorithm for pulse radar systems based on boundary scattering transform,” *IEICE Trans. Commun.*, vol.E87-B, no.5, pp. 1357–1365, 2004.

[5] S. Kidera, T. Sakamoto and T. Sato, “A Robust and Fast Imaging Algorithm with an Envelope of Circles for UWB Pulse Radars”, *IEICE Trans. Commun.*, vol.E90-B, no.7, pp. 1801–1809, July, 2007.

[6] S. Kidera, T. Sakamoto and T. Sato, “High-Resolution and Real-time UWB Radar Imaging Algorithm with Direct Waveform Compensations,” *IEEE Trans. Geosci. Remote Sens.*, vol. 46, no. 11, pp. 3503–3513, Nov, 2008.

[7] S. Kidera, T. Sakamoto and T. Sato, “Accurate UWB Radar 3-D Imaging Algorithm for Complex Boundary without Range Points Connections,” *IEEE Trans. Geosci. Remote Sens.*, (in press).

[8] J. Capon, “High-resolution frequency-wavenumber spectrum analysis,” *Proc. IEEE*, vol. 57, no. 8, pp. 1408–1418, Aug. 1969.

[9] S. Kidera, T. Sakamoto and T. Sato, “A High-Resolution Imaging Algorithm without Derivatives Based on Waveform Estimation for UWB Radars”, *IEICE Trans. Commun.*, vol.E90-B, no.6, pp. 1487–1494, June, 2007.

[10] S. Kidera, T. Sakamoto and T. Sato, “Experimental Study of Shadow Region Imaging Algorithm with Multiple Scattered Waves for UWB Radars,” *Proc. of PIERS 2009*, Vol. 5, No. 4, pp. 393–396, Aug, 2009.